RSC Applied Polymers

ROYAL SOCIETY OF CHEMISTRY

PAPER

View Article Online
View Journal | View Issue

Cite this: *RSC Appl. Polym.*, 2025, **3**, 948

Composition–property engineering of bio-derived UV-curable acrylate oligoester resins for tunable mechanics in 3D printing†

Syed M. Q. Bokhari, [a] Jensen N. Sevening,[b] Jeffrey M. Catchmark[a] and Stephen C. Chmely *[a]

Liquid Crystal Display (LCD) mask projection stereolithography (MPSL) is a 3D printing technology that enables the fabrication of complex, high-resolution structures; however, the mechanical properties of MPSL 3D printed objects are often limited by the resins used. This study focuses on developing and characterizing bio-based polyester UV-curable resins with tunable mechanical properties optimized for MPSL. Bio-based polyester resins were synthesized by direct esterification and a polycondensation reaction of itaconic and/or succinic acids with 1,2-propane-, 1,4-butane-, and/or 1,8-octanediols, followed by blending with triethylene glycol dimethacrylate. The bio-renewable nature of the resin components provides several advantages over traditional petroleum-derived resins. The diacid and diol monomers come from renewable feedstocks such as corn, soybean, and vegetable oils rather than finite fossil fuel reserves. Furthermore, bio-renewable materials lower dependence on petrochemicals and increase the sustainability of 3D printing. The effects of the diacid structure and diol chain length on resin properties were systematically investigated. Chemical characteristics were investigated by NMR and FTIR, suggesting successful synthesis of the desired bio-based polyesters. By varying the molecular design, diacid, and diol building blocks, the molecular weight, crosslink density, and mechanical performance were tailored. The liquid resins were characterized by gel permeation chromatography and rheological measurements, and solid UV-cured objects were characterized by static and dynamic tensile testing. Rheological studies confirmed that all resin formulations displayed shear-thinning behaviour, ideal for MPSL printing. Mechanical testing revealed that varying diacid and diol components could modulate tensile elastic modulus and elongation at break from 0.1 to 1.0 GPa and 3.5 to 8.5%, respectively. Printability was assessed by printing a resolution test structure on a LCD 3D printer equipped with a 405 nm LED source. This ability to tailor the properties of bio-based polyester resins by molecular design provides an avenue for fabricating high-performance MPSL-printed objects targeted for specific applications, ranging from prototypes to end-use products.

Received 28th March 2025,
Accepted 22nd May 2025

DOI: 10.1039/d5lp00085h

rsc.li/rscapplpolym

Introduction

The pursuit of sustainable and environmentally benign manufacturing practices has gained significant momentum in recent years.[1] Vat photopolymerization (VPP), a leading additive manufacturing (AM) platform, has emerged as a transformative technology enabling the fabrication of complex and customized objects with exceptional precision and surface finish.[2,3] VPP is implemented mainly in (i) vector-scanning stereolithography (SLA), where a laser spot is rastered across the resin; (ii) mask-projection stereolithography (MPSL), where an entire layer is polymerised in a single exposure by projecting a digital mask projected with a DMD, LCD, or a related imaging device; (iii) micro-stereolithography (μSL) for meso-scale parts; and (iv) two-photon polymerisation (TPP) for sub-micron features.[4] However, the widespread implementation of these technologies has been hindered by the limited availability of biocompatible and eco-friendly resins derived from renewable resources.[5]

Conventional SLA and MPSL resins are predominantly based on petrochemical-derived acrylates, which raise concerns regarding toxicity and environmental impacts.[6] As a promising alternative, bio-based polyesters have attracted attention due to their hydrolytic degradability, low environ-

[a]*Department of Agricultural and Biological Engineering, The Pennsylvania State University, University Park, Pennsylvania 16802, USA. E-mail: sc411@psu.edu*
[b]*Department of Material Science and Engineering, The Pennsylvania State University, University Park, Pennsylvania 16802, USA*

†Electronic supplementary information (ESI) available: Oligoester composition table, photographs of resins, tensile specimens, 3D printed objects, FTIR and NMR spectra, GPC chromatograms, and rheological plots. See DOI: https://doi.org/10.1039/d5lp00085h

mental footprint, and versatility in tailoring mechanical properties.[7,8] By introducing appropriate UV-curable moieties, these polyesters can be transformed into photo-cross-linkable resins suitable for vat photopolymerization techniques such as SLA and LCD MPSL.[5,9]

Among the myriad polysaccharide-derived renewable resources, itaconic acid and succinic acid have emerged as promising building blocks for synthesizing bio-based polyesters.[10–19] Succinic acid, a dicarboxylic acid produced *via* biomass fermentation, has garnered attention as a sustainable monomer for polyester synthesis.[20] Itaconic acid, a related unsaturated diacid, offers unique functionality and reactivity due to its multifunctional structure.[16]

Recent advancements in the use of bio-based materials for 3D printing have highlighted the increasing potential of sustainable alternatives in additive manufacturing processes. Growing interest in bio-based, biodegradable, and recyclable materials for LCD printing has spurred the development of sustainable photopolymers.[21] Not only that, but significant strides have been made in developing bio-based and environmentally friendly alternatives that maintain high performance.[22] These studies collectively underscore the ongoing shift toward more sustainable practices in 3D printing, with bio-based polyesters emerging as key contributors to this transition.

For example, soybean oil-based methacrylate resins have been developed as a biobased alternative for stereolithography (SLA),[23] offering comparable mechanical properties to their fossil-based counterparts while providing environmental benefits by reducing reliance on petrochemical resources.[24] Similarly, the use of acrylated epoxidized soybean oil in vat photopolymerization has resulted in photocurable resins with high biorenewable content, demonstrating enhanced mechanical and thermal properties suitable for high-performance 3D printing applications.[25] In line with these developments, Cazin *et al.* (2024) proposed a simple synthesis route to bio-based acrylate-modified polyester resins, characterized by their low viscosity, which is ideal for vat photopolymerization in 3D printing. This approach enables the gradual replacement of fossil-based raw materials with bio-based alternatives, further advancing the adoption of environmentally friendly solutions in additive manufacturing.[26]

This study builds on these advancements by addressing the inherent ecological limitations of traditional petroleum-based resins in LCD 3D printing. By focusing on bio-based polyester resins, this work aims to demonstrate their potential to deliver improved sustainability, reduced environmental impact, and tuneable material properties. This shift toward bio-based alternatives represents a significant step forward in the pursuit of more sustainable and innovative solutions in additive manufacturing, underscoring the relevance of this research.

For example, polybutylene succinate (PBS), a commercially viable bio-based polyester derived from succinic acid and 1,4-butanediol, has demonstrated promising properties and biodegradability.[19] Incorporating itaconic acid and other sustainable diols, such as 1,2-propanediol and 1,4-butanediol,[27] presents an opportunity to engineer tailored mechanical properties suitable for SLA and LCD 3D printing applications.[21,22] On the other hand, the resulting materials will overall have substantially lowered biodegradability due to their highly crosslinked network structure imparted by the presence of itaconic acid. In any case, several recent examples that employ itaconic acid to create photocrosslinkable resins for 3D printing exist.[17]

For example, Carmenini and coworkers demonstrated that biobased urethanediol itaconates could be 3D printed to create objects with elastic moduli as high as 1 GPa and tensile strengths exceeding 30 MPa.[28] In addition, Vetri Buratti and coworkers demonstrated that a series of poly(ester amide) materials consisting of itaconic acid, vanillic acid, and a diamide synthesized from caprolactone and butanediamine displayed a variety of tensile moduli (50–85 MPa) and tensile strengths (4–5 MPa), and these materials elicited no cytotoxic response from human keratinocytes.[29] Maturi and coworkers showed that phosphorescent bio-based resins containing oligoesters consisting of itaconic acid, propanediol, glycerol, and vanillic acid had a tensile modulus of 62 MPa and an ultimate tensile strength of 5.4 MPa.[30] In another contribution, Maturi and coworkers created methacrylate-free bio-derived photocurable resins containing itaconic acid and thioesters derived from limonene, linalool, and geraniol that showed a wide range of storage moduli (400–1200 MPa).[31] Finally, Papadopoulos and coworkers created itaconic acid-based 3D printed nanocomposites and showed that a variety of nanoscale reinforcing agents could enhance the elastic modulus and ultimate tensile strength of printed objects by more than double (600 MPa to 1520 MPa using cellulose nanocrystals).[32]

Systematic variation of the diacid and diol components allows structure–property relationships governing mechanical performance to be effectively elucidated. UV-curing AM is based on the principle of targeted UV-light emission on photocurable materials. However, several parameters affect the processability of such materials, such as viscosity and reactivity towards UV-light-induced crosslinking.[33–35] To render polymers suitable for AM, a common strategy is to utilize reactive diluents to create formulations with viscosities needed for the respective printing process.[36] Besides the role of the reactive diluent in reducing the viscosity, it also influences both reactivity towards UV-light-induced photocuring and the final material properties. Furthermore, reactive diluents allow for higher double bond conversion, as more crosslinking reactions can occur in formulations with lower viscosity before vitrification takes place and the mobility of the polymer chains is suppressed.[37,38] We further hypothesized that systematic substitutions of the monomers, including itaconic acid, succinic acid, and diols such 1,8-octanediol, 1,4-butanediol, and 1,2-propanediol, would afford measurable and controllable structure–property relationships governing the mechanical performance of the resulting cured resins.

In this study, we investigated the effects of diacid and diol monomers on the mechanical properties of liquid resins and cured solid objects, such as tensile strength, crosslink density, and Young's modulus. We seek to identify optimal combi-

nations that yield bio-based oligomeric polyester UV-curable resins with tailorable mechanical characteristics. These insights will contribute to expanding the range of environmentally friendly materials available for SLA/MPSL 3D printing and enable the production of functional and sustainable objects with tailored mechanical performance.

Experimental

Materials

2,5-Bis(5-*tert*-butyl-benzoxazol-2-yl)thiophene (UV blocker, 99%), 1,4-butanediol (1,4-BDO, 99%), diphenyl(2,4,6-trimethylbenzoyl) phosphine oxide (TPO, 97%), itaconic acid (IA, 99%), methanol (99.8%), 4-methoxyphenol (MeHQ, 99%), and triethylene glycol dimethacrylate (TEGDMA, 95%) were obtained from MilliporeSigma (Burlington, MA USA). Phenolphthalein indicator (ACS grade), potassium hydroxide (KOH, reagent grade), 1,2-propanediol (1,2-PDO, 99.5%), and succinic acid (SA, high-purity) were obtained from VWR International (Radnor, PA USA). 1,8-Octanediol (1,8-ODO, high-purity) was obtained from Biosynth International, Inc. (Gardner, MA USA). Acetone and tetrahydrofuran (THF) were obtained from Fisher Scientific International, Inc. (Pittsburgh, PA USA) and were of ACS grade or better. Ethanol (190 proof) was obtained from Decon Laboratories (King of Prussia, PA USA). All reagents were used as received unless specified otherwise. Dimethyl sulfoxide-D6 (DMSO-D6, 99%) was obtained from Cambridge Isotope Laboratories, Inc. (Tewksbury, MA USA) and was stored over anhydrous calcium sulphate prior to use.

Photoactive oligoester synthesis and characterization

Unsaturated oligoesters were synthesized using a direct esterification polycondensation reaction with 45% excess hydroxyl groups (diacid to diol ratio of 1 : 1.45), which facilitates a low degree of polymerization. The synthesized resins were classified into three distinct classes of resin formulations by varying diols. In classes A, B, and C, different ratios of itaconic acid and succinic acid were reacted with 1,2-PDO, 1,4-BDO, and 1,8-ODO, respectively. The full matrix of sample IDs can be found in the ESI.† A representative preparative scheme is described in detail below.

For the preparation of the 50 : 50 oligoester of class A, a 125 mL round-bottom flask equipped with a magnetic stirrer was charged with 6.5 g of IA (0.050 mol, 0.50 eq.), 5.9 g of SA (0.050 mol, 0.50 eq.), and 11.0 g of 1,2-PDO (0.145 mol, 1.45 eq.). The flask was stirred at 300 RPM and heated to 165 °C using an oil bath. After 15 minutes, to ensure complete melting of the monomers, the temperature was reduced to 145 °C and the reaction was allowed to proceed for an additional 2 hours and 45 minutes. The reaction was then allowed to cool to room temperature.

Progress to completion (% completion) was measured by titrating the oligoester samples using KOH to determine the amount of remaining carboxylic acids using the protocol outlined in ASTM D7253. The chemical structure of each oligoester was characterized using NMR and FTIR spectroscopy methods. ^{1}H NMR spectra were recorded at 25 °C using a Bruker Avance III 500 MHz spectrometer. Chemical shift values are reported in ppm (δ). Fourier transform infrared (FT-IR) spectra were recorded using a Bruker Vertex 70 spectrometer equipped with a liquid nitrogen-cooled mid-band mercury cadmium telluride (MCT) detector. Spectra were recorded in attenuated total reflection (ATR) geometry under nitrogen purging using a Harrick DiaMax diamond ATR accessory at an incident angle of 45°. A total of 400 scans were averaged at 4 cm^{-1} resolution, and absorbance was calculated by referencing the clean bare diamond crystal.

The molecular weight distribution of each oligoester class was determined using gel permeation chromatography (GPC). GPC measurements were conducted at 40 °C on a Tosoh EcoSEC with an RI detector using tetrahydrofuran (THF) as the eluent. Poly(methyl methacrylate) (PMMA) was used as a standard to calibrate the instrument in the range of 690 Da to 0.4674 MDa. Samples were dissolved in THF (5 mg mL^{-1}) and filtered over a 0.2 mm PTFE syringe filter prior to injection.

Resin formulation and characterization

Photocurable resins (20 g each) were prepared by mixing 50% (w/w) photoactive oligoester, 47% (w/w) TEGDMA (reactive diluent), and 3% (w/w) TPO (photoinitiator). The as-prepared resins were introduced to a 20 mL glass scintillation vial and stored in a dark place prior to characterization and use. 3D printable LCD-MPSL resins also contained 0.16 wt% of 2,5-bis (5-*tert*-butyl-benzoxazol-2-yl)thiophene (UV blocker). All rheological measurements were performed on a strain-controlled Discovery HR-3 rheometer equipped with a cone-plate geometry with a diameter of 40 mm, a gap of 0.043 mm, and a cone angle of 2 degrees. Measurements were made for 180 s at 20 °C. Scheme 1 shows the molecules used in this study and a potential network consisting of these monomers.

Thermoset formation and characterization

Tensile testing specimens were prepared by pouring the resins into flexible silicone moulds and subsequently cured for 1 min with a 400 W metal halide UV lamp (Uvitron International, Inc., West Springfield, MA, USA) with an irradiance of 200 mW cm^{-2}. Each mould had dimensions appropriate for static (type-V tensile testing dogbone from ASTM-D638[39]) or dynamic mechanical testing.

The degree of double bond conversion (DC) was determined by FT-IR to obtain the peak ratio of the C=C bond to a peak that remains unchanged in both the post- and pre-polymer and to compare the two using eqn (1):[40]

$$\mathrm{DC}\,(\%) = \left[1 - \frac{\dfrac{A_{\mathrm{C{=}C_{post}}}}{A_{\mathrm{std_{post}}}}}{\dfrac{A_{\mathrm{C{=}C_{pre}}}}{A_{\mathrm{std_{pre}}}}}\right] \times 100\% \qquad (1)$$

where $A_{\mathrm{C{=}C}}$ is the area of the C=C peak at 1638 cm^{-1} and $A_{\mathrm{std_{pre}}}$ and $A_{\mathrm{std_{post}}}$ are the areas of the internal standard peak selected for the pre- and post-polymer, respectively. Spectra

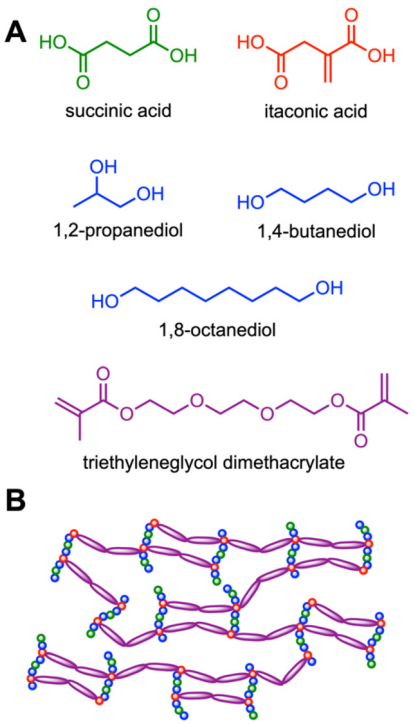

Scheme 1 Molecules used in this study (a) and the potential crosslinked network (b).

were baseline-corrected using a two-point method and normalized to the C=O peak prior to the calculation of the degree of double bond conversion (DC).

Gel fraction (F_{gel}) was determined *via* extraction of the remaining free oligomers from the crosslinked polymer. Rectangular polymer samples weighing approximately 0.12 g were incubated in acetone (20 mL per sample) under mild shaking at room temperature for 24 h, followed by vacuum drying at 40 °C for 48 h to remove the residual solvent. F_{gel} (%) was calculated as the quotient of the final and initial sample weights.

Static tensile testing was conducted using an MTS Criterion load frame (MTS Systems, Eden Prairie, MN, USA) equipped with a load cell featuring a nominal force capacity of 5 kN. An MTS Bionix Scissors Action grip was employed to securely hold the dogbone specimens during testing. The testing rate was set at 1 mm min^{-1} to simulate controlled tension conditions. An MTS Advantage Video Extensometer was used for non-contact measurements of mechanical response with typical displacement resolutions of 0.13 μm and an image capture frequency ranging from 0.1 to 30 Hz. The minimum measurable strain values were established at 0.01%. Two black stripes were made with a permanent marker at the top and bottom of the narrow part of the dogbone to track the strain during the test. Young's modulus for the samples was determined within the strain range of 0.5 to 1%. For each sample among classes, a total of 10 samples were measured, and an average value of elongation at break, ultimate tensile strength, and Young's modulus was calculated to ensure statistical reliability and robustness in the reported results.

Dynamic mechanical analysis (DMA) was carried out on a TA Instruments Q800 dynamic mechanical analyser (TA Instruments, New Castle, DE, USA) in tension (film/fibre) mode. Measurements were performed on rectangular bars (dimensions: 25 mm × 5 mm × 1.5 mm) prepared *via* mould casting as above. Sample analysis was performed in air at a temperature range of 40 to 210 °C with a heating rate of 5 °C per minute at a frequency of 1 Hz with a maximum displacement of 15 μm. Exact specimen dimensions were determined before each experiment with a digital calliper.

Crosslink density (ν) was calculated according to the following equation:

$$\nu = \frac{\rho}{M_c} = \frac{E'}{3RT} \quad (2)$$

where E' is the storage modulus in the rubbery state, R is the universal gas constant (8.3144 J mol^{-1} K), and T is the absolute temperature (K) in the rubbery state.

To quantify any thermal contribution during photopolymerization, an ASTM D648 type V dogbone of PDO resin (100 : 0 IA : SA) was cured under a 500 W metal–halide lamp (200 mW cm^{-2}) for 60 s. Surface temperature was recorded every 10 s using an infrared thermometer.

3D printing was conducted on an Elegoo Mars 2 Pro LCD-MPSL printer (Elegoo, Shenzhen, Guangdong 518110 China) equipped with an LED array (405 nm). Several resolution test structures were 3D printed with a layer thickness of 20 μm and an exposure time of 10 s per layer with a bottom exposure time of 35 s. After printing, samples were removed from the printer and submerged in a cleaning bath of 70% ethanol for 30–45 seconds. They were then air-dried and removed from the build platform.

Statistical analyses

All the experimental sample data were reported as a mean ± standard error of the mean. Unless stated otherwise, the value of n is defined as the number of repetitions of the sample group. Statistical analysis was performed using a one-way analysis of variance (ANOVA). A Tukey or Tukey–Kramer test was used to compare means and differences. Values with $p < 0.05$ were considered statistically significant. All statistical analyses were performed using MINITAB 19.0 (Minitab LLC., State College, PA, USA).

Results and discussion

Synthesis and characterization of oligoesters

We synthesized a series of oligoesters *via* solvent-free direct polycondensation of diacids and diols using a diacid-to-diol ratio of 1 : 1.45. The melt polycondensation approach enabled the solvent-free, single-step preparation of UV-curable oligomeric oligoesters. A structural example of the PDO-containing oligoester is shown in Scheme 2; the other oligoesters would have analogous structures with BDO and ODO. A large excess of diol was employed to ensure low degrees of polymerization,

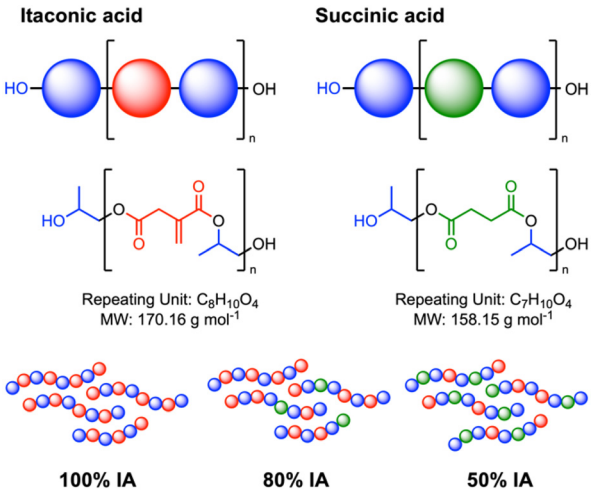

Scheme 2 Repeating units of the PDO oligoester containing 1,2-propanediol (blue) and a controllable mixture of itaconic acid (red) and succinic acid (green).

which we hypothesized could afford ideal viscosity profiles for VAT photopolymerization techniques. In addition to the variation of the monomers, crosslink density defines the properties of thermosetting polymers. Accordingly, we varied the itaconic acid content among the prepared polyesters, resulting in materials of different double bond densities (DBD).

We measured the percent completion of each polycondensation by titration with KOH and tabulated the results in the ESI.† In short, due to the relatively short reaction times (3 h), none of the reactions reached 100% completion, although they ranged from 76% completion for the PDO oligoesters to over 90% completion for the ODO oligoesters. We attribute this to a complex combination of steric hindrance and chemical reactivity. In the case of 1,2-propanediol, there is much greater steric congestion for diacids to react than in the case of 1,8-octanediol, leading to a slower progress to completion for a given reaction time. In addition, itaconic acid is partially conjugated, and therefore, the acidity of the carboxylic acid group proximal to the methylene will be lower than that of the distal carboxylic acid. Moreover, those will be different from the acidity of the equivalent carboxylic acid groups in succinic acid. In any event, the oligoesters we isolated show interesting solubility and molecular weight features that we discuss in greater detail below, which afford the mechanical properties that we desire.

We employed ATR-FTIR spectroscopy for chemical characterization of the synthesized polyester resins. Representative spectra for PDO oligoesters are shown in Fig. 1. FTIR spectra for all other classes can be found in the ESI.†

As shown in Fig. 1, all oligoesters exhibited a distinctive peak at 1635 cm^{-1} corresponding to the C=C stretching vibration, confirming the successful incorporation of carbon–carbon double bonds from the itaconic acid monomers. Additional peaks related to the ester linkages are also present, including those at ~1708, ~1192, and ~1145 cm^{-1} from the C=O, C–C–O, and O–C–C stretching vibrations, respectively. The peak frequencies shift with increasing amounts of SA owing to the changes in the ester linkages among SA esters and IA esters. We were also able to detect FTIR frequencies for unreacted carboxylic acid groups (ν = 2977 cm^{-1}) owing to the short reaction times we employed (3 h total) to synthesize each oligoester.

FTIR spectroscopy could be unreliable in discriminating between the incorporation of itaconic acid and its perhaps less

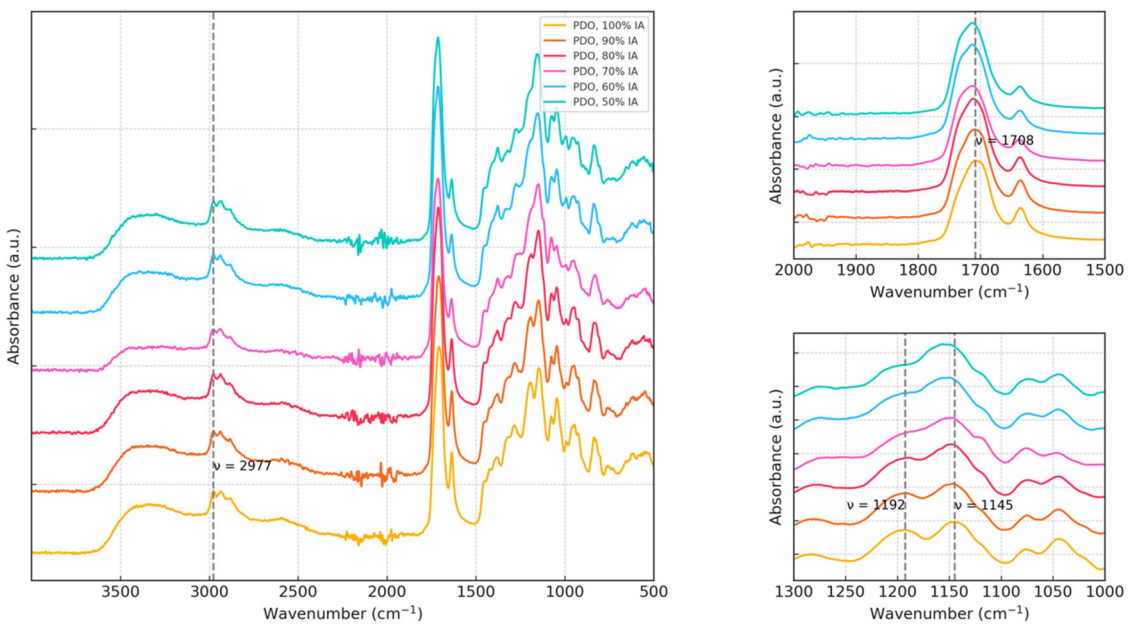

Fig. 1 ATR-FTIR spectra of PDO oligoesters containing 50–100% itaconic acid with a balance of succinic acid. Inset plots for the wavenumber ranges of 2000–1500 cm^{-1} and 1300–1000 cm^{-1} are included.

useful isomer 2-methyl-2-butenedioic (mesaconic) acid, whereas NMR spectroscopy could unambiguously determine the presence (or absence) of these monomers. Representative ^{1}H NMR spectra for BDO oligoesters are shown in Fig. 2. NMR spectra for all other classes can be found in the ESI.†

As shown in Fig. 2, signals attributable to vinylic protons are present (I_1 and I_2 in Fig. 2), indicating that the side-chain double bond remains intact during the synthesis process and implying that it is available for further crosslinking during UV-induced radical curing. Under certain synthesis conditions, the C=C double bond from itaconic acid can isomerize to form mesaconic acid, which can lead to a significant decrease in the reactivity of the polyesters during photopolymerization. However, no signals corresponding to mesaconic acid could be detected in any of the NMR spectra.

Instead, the methylene protons of the itaconate units are present in all the collected NMR spectra. Likewise, the ester linkage protons that confirm the successful synthesis are present in all spectra. Ester protons on the diol chains (B_{Est} in BDO as shown in Fig. 2) are magnetically inequivalent because of the molecular asymmetry of IA, which adds some complexity to the resulting spectra. However, the single downfield ester peak grows as more SA is present, reflective of the molecular symmetry of SA. Unsurprisingly, no resonance signals from the free –OH groups of the terminal hydroxy groups were observed. Peaks related to succinic acid (S_1 in Fig. 2) appeared as the amount of SA relative to IA increased. However, all peaks were observed and assignable to each NMR spectrum (see the ESI† for additional spectra for PDO- and ODO-containing samples).

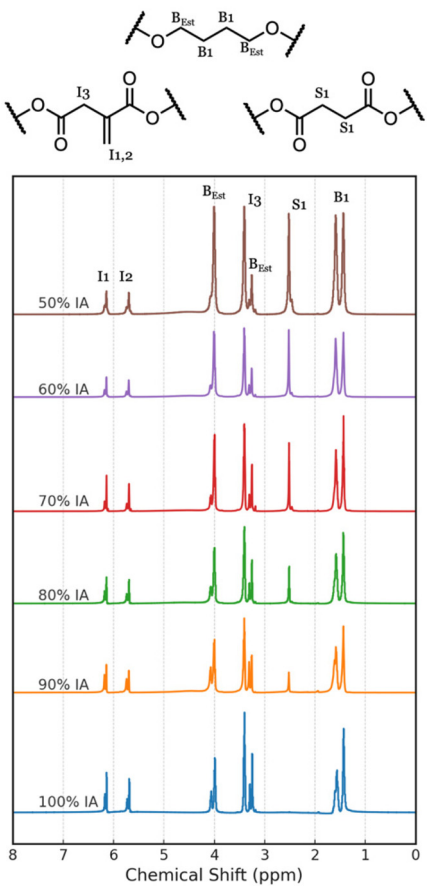

Fig. 2 ^{1}H NMR spectra of BDO oligoesters containing 100–50% IA with a balance of SA.

Table 1 Molecular weight of the synthesized oligoesters

Class	IA : SA	M_n [a]	M_w [a]	$Đ$	MW of RU [b]	DP [c]
PDO	100 : 0	798	988	1.24	170.16	4.69
	90 : 10	780	957	1.23	168.96	4.62
	80 : 20	876	1080	1.23	167.76	5.22
	70 : 30	921	1155	1.25	166.56	5.53
	60 : 40	954	1188	1.25	165.36	5.77
	50 : 50	977	1219	1.25	164.16	5.95
BDO	100 : 0	804	1058	1.32	184.19	4.37
	90 : 10	907	1165	1.28	182.99	4.96
	80 : 20	937	1193	1.27	181.79	5.15
	70 : 30	890	1109	1.25	180.59	4.93
	60 : 40	934	1180	1.26	179.39	5.21
	50 : 50	874	1111	1.27	178.19	4.91
ODO	100 : 0	731	973	1.33	240.30	3.04
	90 : 10	754	1000	1.33	239.10	3.15
	80 : 20	822	1078	1.31	237.90	3.46
	70 : 30	807	1062	1.32	236.70	3.41
	60 : 40	859	1121	1.31	235.50	3.65
	50 : 50	854	1116	1.31	234.30	3.64

[a] Determined by SEC, g mol^{-1}. [b] Computed molecular weight (g mol^{-1}) of a hypothetical average bimolecular repeating unit (RU, see Scheme 2) for a given diol and a mixture of itaconic acid (IA) and succinic acid (SA). [c] Degree of polymerization (DP), computed as the quotient of the measured M_n and MW of the given RU.

We employed gel permeation chromatography to measure the molecular weight distributions of the as-synthesized oligoesters. A chromatogram for each oligoester can be found in the ESI.† The molecular weight data are summarized in Table 1.

Overall, oligoesters for each class have a degree of polymerization (DP) in the range of 3–6. These values agree generally well with a computed maximum DP of 3.44 based on the Carothers equation for a polyester system with the amount of diol being 45% excess.[41] The exact reasons for these variations are unknown but are potentially attributable to variations in reagent purity and/or progress to completion for each reaction as discussed above. Moreover, the Carothers equation is known to assume constant reaction kinetics and ignore intramolecular interactions,[42] both of which potentially play a role in synthesizing oligoesters using diols and diacids with varied steric pressures and rates of reactivity. Nonetheless, these results agree well with theory and demonstrate that we were able to synthesize oligoesters having DP = 3–6. However, the molecular weight data are generally bimodally distributed, owing to the short reaction times employed.

Thermoset formation *via* curing in moulds

Resins were blended as mixtures of TEGDMA, TPO, and a suitable oligoester. We hypothesized that the multifunctional TEGDMA molecules would crosslink the oligoesters when exposed to UV light (Scheme 1). We fabricated several silicone molds to obtain samples for both static and dynamic mechanical analyses. Photographs of these molds are provided in

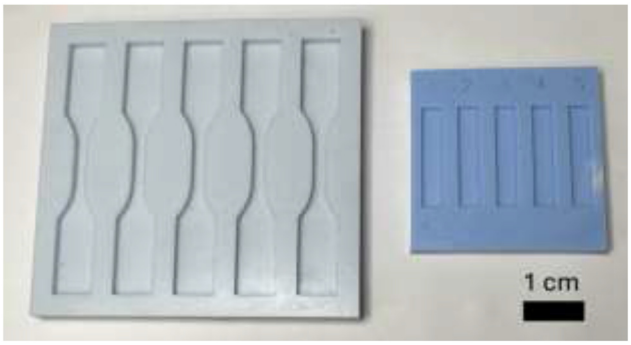

Fig. 3 Photographs of the molds used to create photopolymerized thermosets. Samples were used to conduct static (left) and dynamic (right) mechanical analyses.

Fig. 3. The as-mixed resins are translucent, and the Hg vapor lamp we employed has a relatively high flux, so light was able to penetrate through the samples to the back side of the mold and completely cure each sample. We did not note any uncured resin on any samples. Photographs of all the resins and cured dogbones are provided in the ESI.†

Gratifyingly, the oligoesters we synthesized are readily soluble in our reactive diluent TEGDMA. We attempted to drive a reaction to completion in the manner described by Robert and coworkers.[32] However, the material we synthesized at 18 h at 160 °C was insoluble in TEGDMA. In the referenced case, the group used 4-acryloylmorpholine (ACMO) as a monofunctional diluent, which could be why their samples completely dissolved at long reaction times.

We hypothesized that the molecular structure of the diacid and diol components in the synthesized oligoesters can influence the mechanical properties of the crosslinked polymer. Modulation of the amount of itaconic acid and the length of the diol chain in the synthesis can allow the fine-tuning of the crosslink density and, consequently, the mechanical properties (Scheme 2). The incorporation of itaconic acid with its carbon–carbon double bonds within the polymeric backbone imparts unique structural and functional attributes that can be exploited to modulate material properties. The double bond density (DBD) strongly governs the physicochemical characteristics of the polymer network after photocuring, since the presence of pendant C=C sites enables subsequent crosslinking *via* free radical propagation while also reducing rotational freedom along the backbone. Higher DBD values typically lead to more densely crosslinked and therefore stiffer networks, although embrittlement can occur at very high concentrations. Similarly, short-chain diols, such as 1,2-PDO, can lead to higher crosslink densities, resulting in stiffer and stronger polymeric networks. Conversely, longer-chain diols, such as 1,8-ODO, will produce more flexible networks with lower tensile strengths and moduli due to the increased spacing between the crosslink junctions. By tuning DBD during oligoester synthesis through our molecular design technique, a wide variety of resin formulations with varying strength and stiffness values was targeted. Fig. 4 provides a graphical representation of various mechanical properties across all specimens as determined using static tensile testing. Moreover, Table 2 provides a numerical summary of those mechanical properties.

As shown in Fig. 4 and summarized in Table 2, there are obvious trends in the mechanical properties as a function of diol and IA : SA ratio. For example, for PDO and BDO, decreasing IA leads to a decrease in DBD, which manifests as a decrease in both strength and stiffness. This is an important result, as it demonstrates that the mechanical properties are controllable by changing the amount of IA in the formulation. Fewer IA molecules overall lead to fewer crosslinkable C=C bonds (Scheme 2), which leads to a decrease in strength and stiffness. This also evidently affords an increase in ductility as demonstrated by an increase in elongation at break.

However, there is not an appreciable change in tensile strength for ODO samples. Moreover, the measured values for

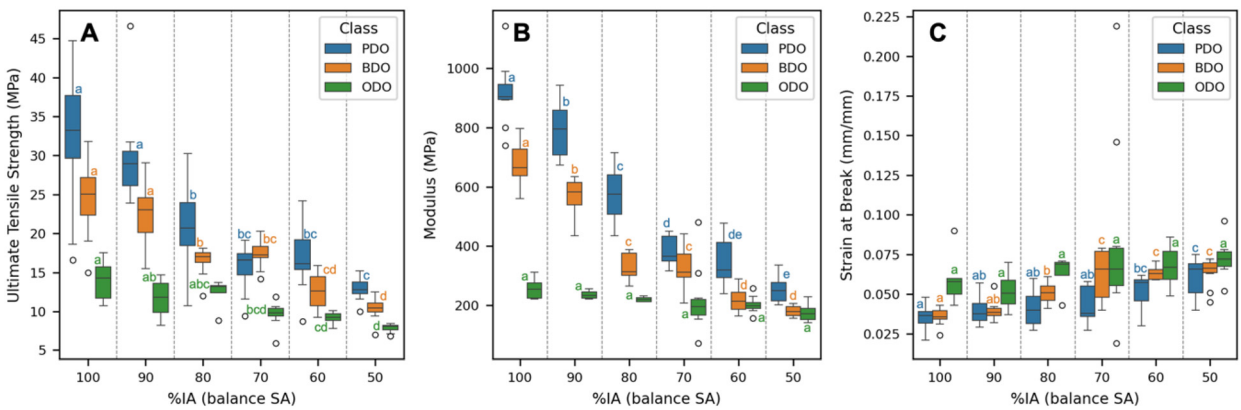

Fig. 4 Category plots of the results of static tensile tests. Shown are the ultimate tensile strength (UTS, A), Young's modulus (B), and strain at break (C) for PDO (blue), BDO (orange), and ODO (green) samples having the listed percentage itaconic acid (IA) and a balance of succinic acid (SA). Each measurement was conducted ten times. The bars display the maximum and minimum values, and the upper and lower quartiles are enclosed in the boxes. The horizontal line denotes the median (not the mean), and any outliers are displayed as open circles. Color-coded letters denote the results of a Tukey pairwise test of honest significant differences. Mean values (displayed in Table 2) that are not statistically different share letters.

Table 2 Static mechanical properties of ASTM dogbone specimens

Class	IA : SA	UTS (MPa)	Young's modulus (MPa)	Elongation at break (%)
PDO	100 : 0	32.4 ± 2.9	916 ± 34	3.49 ± 0.24
	90 : 10	29.9 ± 2.0	790 ± 30	3.89 ± 0.27
	80 : 20	21.0 ± 1.8	573 ± 27	4.14 ± 0.38
	70 : 30	15.6 ± 1.1	379 ± 16	4.34 ± 0.38
	60 : 40	16.8 ± 1.4	348 ± 24	5.17 ± 0.34
	50 : 50	12.86 ± 0.46	254 ± 14	6.00 ± 0.40
BDO	100 : 0	24.2 ± 1.5	679 ± 22	3.58 ± 0.18
	90 : 10	22.4 ± 1.2	571 ± 19	3.97 ± 0.20
	80 : 20	16.33 ± 0.63	333 ± 15	5.07 ± 0.21
	70 : 30	17.27 ± 0.61	321 ± 23	6.27 ± 0.52
	60 : 40	12.63 ± 0.74	220 ± 13	6.32 ± 0.13
	50 : 50	10.43 ± 0.50	181.4 ± 5.8	6.39 ± 0.28
ODO	100 : 0	14.0 ± 1.3	258 ± 17	6.02 ± 0.80
	90 : 10	11.6 ± 1.4	236.8 ± 7.9	5.20 ± 0.70
	80 : 20	12.28 ± 0.90	221.2 ± 3.9	6.30 ± 0.52
	70 : 30	9.63 ± 0.49	218 ± 35	8.4 ± 1.8
	60 : 40	9.17 ± 0.24	202.3 ± 8.6	6.77 ± 0.38
	50 : 50	7.83 ± 0.17	176 ± 10	7.24 ± 0.35

Young's modulus and elongation at break for ODO are not statistically different. The overall lower stiffness and strength values for ODO when compared to PDO and BDO samples are perhaps unsurprising, as these networks are likely much more flexible owing to the longer diol chain length (8 carbons in ODO *versus* 4 in BDO and 2 in PDO). However, it appears that an ability to control the mechanical properties by changing the IA : SA ratio in ODO polymers is for whatever reason largely diminished when compared to PDO and BDO. Nonetheless, we could access a wide range of modulus values, from a few hundred MPa to nearly 1 GPa, by altering the diol chain length and crosslinkable C=C double bonds. Our highest-strength formulation of PDO resin at an IA : SA ratio of 100 : 0 delivers 32 MPa tensile strength, more than three times that of vegetable-oil vitrimers (≤9 MPa)[43] and approaching 45 MPa reported for fully biobased acrylates by Miao *et al.*,[44] confirming that a higher double-bond density directly enhances load-bearing performance.

We also quantified the crosslink density ν of the solid objects using both DMA and measurements of gel fractions. Those data are summarized in Table 3. Full DMA curves for each sample are provided in the ESI†.

The extent of crosslinking significantly influences the mechanical performance, dimensional stability, and solvent resistance of photocured resins. Crosslink density provides a quantitative measure of the concentration of interconnected covalent bonds within the polymerized network. As expected, crosslink density decreased as the amount of IA decreased within diol samples. The high crosslink density likely contributes to enhanced stiffness, strength, and thermal stability due to the reduced molecular mobility. In contrast, the sparsely crosslinked networks enable greater elongation and resilience as polymer chains can readily slide past one another without fracture. By tailoring the diacid and diol precursors, UV-cured polyesters with widely varying crosslink densities were successfully developed to meet the broad mechanical property requirements of SLA-printed components.

Table 3 Dynamic mechanical properties of solid rectangular samples

Class	IA : SA	$E'_{40\,°C}$ [a] (MPa)	$E'_{rubbery}$ [b] (MPa)	T_g [c] (°C)	F_{gel} [d] (%)	ν [e] (μM)
PDO	100 : 0	1781	57	137	102.8 ± 0.9	5.0
	90 : 10	1597	51	134	104.0 ± 1.4	4.5
	80 : 20	1606	45	131	103.9 ± 0.8	4.0
	70 : 30	986	30	116	88.8 ± 1.5	2.6
	60 : 40	611	37	105	79.3 ± 1.1	3.2
	50 : 50	382	17	96	75.4 ± 0.6	1.5
BDO	100 : 0	1013	113[f]	140	103.8 ± 1.4	9.5[g]
	90 : 10	1183	99[f]	123	104.7 ± 0.9	9.4[g]
	80 : 20	941	68[f]	111	103.0 ± 2.3	6.4[g]
	70 : 30	617	39[f]	96	93.0 ± 1.1	3.7[g]
	60 : 40	408	25[f]	84	84.8 ± 0.7	2.4[g]
	50 : 50	364	32[f]	93	81.7 ± 0.6	2.9[g]
OD	100 : 0	447	41	98	94.4 ± 0.5	3.6
	90 : 10	461	35	92	91.8 ± 0.2	3.0
	80 : 20	326	35	93	86.0 ± 0.8	3.1
	70 : 30	260	22	94	81.0 ± 1.4	2.0
	60 : 40	261	20	93	81.4 ± 1.9	1.9
	50 : 50	173	14	103	72.4 ± 0.5	1.2

[a] Storage modulus measured at 40 °C by DMA. Full DMA curves are provided in the ESI.† [b] Storage modulus measured at the rubbery plateau by DMA. Measurements were taken from the rubbery plateau at 170 °C unless noted otherwise. [c] Glass transition temperature reported as the peak of tan delta by DMA. [d] Gel fraction reported as the average ± standard error for $n = 3$. Values above 100% are likely a result of the inherent error in measurements and the corresponding samples should be considered completely crosslinked. [e] Crosslink density (ν, micromolar, μM) computed using eqn (2). [f] Storage modulus measured at 150 °C due to decomposition in DMA. [g] Crosslink density computed using storage modulus measured at 150 °C.

Despite a lower Young's modulus as measured by static tensile testing (Fig. 4), BDO samples display a higher ν when compared to PDO samples for the same IA : SA ratio. We attribute this to a thermal decomposition of the BDO samples in the DMA instrument (see related DMA plots in the ESI†). Because of this, the rubbery plateaus for these samples did not extend to 170 °C, so we report $E'_{rubbery}$ at 150 °C instead. Consequently, we caution the reader that comparing PDO, BDO, and ODO is not instructive. However, the trend within samples that less IA leads to a lower ν value does hold as expected.

We quantified the thermal profile during curing and confirmed that the brief heat pulse has no practical effect on network formation. A silicone mold of an ASTM D648 type V dogbone of PDO resin with a 100 : 0 IA : SA ratio was exposed for 60 s under a 500 W lamp while the surface temperature was recorded every 10 s with an IR thermometer. As detailed in Table 4, the sample surface reaches 58 °C within the first 10 s and plateaus at ~97 °C after 50 s of full-power irradiation.

The literature shows that comparable unsaturated-polyester and isocyanate–acrylate systems require ≥ 100 °C for many minutes to achieve even partial thermal cure. Rahmat and Day observed only the onset of curing at 90 °C and needed 25–40 min at 110–150 °C for full conversion,[45] while Studer *et al.* reported just 50% conversion after 4 h at 90 °C, reaching completion only after 2 h at 130 °C.[46] Thus, the transient sub-100 °C thermal dose in our protocol cannot contribute mean-

Table 4 Surface temperature of a PDO (100 : 0 IA : SA) resin during UV curing

Time (s)	Temperature (°C)
0	33
10	58
20	76
30	89
40	94
50	97
60	98

ingfully to network formation, confirming that curing is governed by photopolymerization alone.

A typical strategy to determine the degree of double bond conversion (DC) *via* FT-IR is to assign the 1638 cm^{-1} C=C band as an internal reference that is invariant both before and after curing and compare the two spectra. In some cases, an internal reference is easily obtainable; for example, a C–H, aromatic C=C, or C–O vibration can be used as an internal standard.[40,47]

In our case, however, there is a significant overlap of peaks from acids, TEGDMA, and the various diols used in this study. As a result, peaks that would ordinarily be good candidates for internal standards change in intensity during polymerization (see the ESI†). The best option we identified is the C=O peak at 1723 cm^{-1}, which is predominantly ascribed to TEGDA C=O (1715 cm^{-1}), with some overlap from acid and ester C=O, resulting in the broadening of the peak compared to pure diacrylate (see the ESI†). This peak is routinely used as an internal standard for simpler diacrylate systems to measure the degree of double bond conversion.[48] The apparent shift of this peak in our system after crosslinking, from 1713 cm^{-1} to 1718 cm^{-1}, is due to the conversion of acid C=O (1678 cm^{-1}) to ester C=O (1745 cm^{-1}). The degree of conversion determined by this method ranged from 40% to 77%; the full set of values is presented in a table in the ESI.†

The gel fraction denotes the portion of the insoluble network formed during photo-induced free radical polymerization and crosslinking of the functionalized polyester resins. This parameter provides a valuable measure of attainable oligomeric polymer-to-crosslinked polymer conversion and the associated development in mechanical integrity. The measured gel fractions exceeded 72% for all resin formulations, demonstrating high C=C bond conversion and progressive vitrification during UV irradiation. The dense, rigid samples containing PDO showed near quantitative conversion of the polyester precursor to an infusible solid. The flexible resins containing ODO displayed somewhat reduced gel fractions around 72–94%, likely due to the increased oligomer chain length and content, which can dissolve during swelling. Gel fractions of less than 100% indicate the presence of crosslinked material owing to the presence of incompletely incorporated chains containing, for example, only succinic acid, which will not participate in photocrosslinking and could dissolve as part of the sol fraction. This agrees with our strategy of driving the reactions to lower than 100% completion (see above) and is demonstrated by the increase in sol fraction with respect to an increase in succinic acid content.

Our thermosets reach gel fractions above 72% even though ATR-FTIR shows only 40–70% vinyl conversion. This mismatch is inherent to how densely functional acrylates cure. An infinite, solvent-insoluble network forms as soon as roughly one-quarter of the C=C groups react. Continued exposure drives the network past its glass-transition temperature; vitrification halts diffusion of radicals and chain segments, trapping the remaining vinyl groups that FT-IR still detects.[49]

This rapid, early gelation is not a drawback but a prerequisite for vat photo-polymerization additive manufacturing, where each printed layer must solidify within seconds to preserve dimensional accuracy and support the next layer. The formulations are thus engineered for fast network formation, accepting some residual unsaturation to meet the demands of high-speed printing while delivering mechanically robust, fully insoluble parts.

3D printing by LCD-MPSL

The high gel fractions verify suitable reactivity and sufficient UV exposure to achieve near-complete conversion into insoluble crosslinked structures necessary for application as LCD printing resins. We further investigated the rheological properties of the as-prepared resins, since resin viscosity is an important parameter in 3D printing applications.

Shear viscosity measurements performed at 20 °C from 1 to 1000 s^{-1} indicated shear-thinning profiles for all resins with viscosities below 5 Pa s across the range (see the ESI†). The decreasing viscosity with the increasing shear rate facilitates flow during recoating between successive LCD fabrication layers. Newtonian plateaus at low shear arise from entanglement forces, while shear alignment and disentanglement of chains cause viscosity reduction at higher shear rates.

Finally, we fabricated a printing resolution test using the rigid 100 : 0 IA : SA PDO resin. We chose the 3D printing "torture test" shown in Fig. 5 because it contains several challenging geometries to resolve, including bridges, rounded features, negative features, and overhangs. We also printed

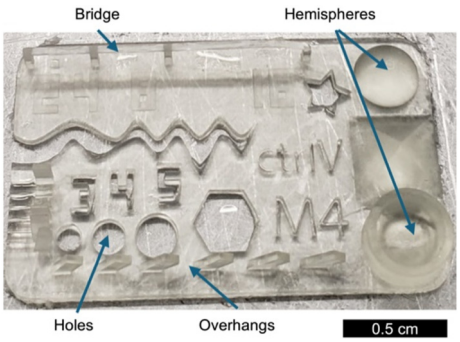

Fig. 5 Photography of the "torture test" 3D printed using the rigid 100 : 0 IA : SA PDO resin.

several resolution tests with varying exposure times to qualitatively analyze relationships between resolution and exposure time (see the ESI†). For engineering context, the key mechanical and printing parameters of four commercial LCD-MPSL resins are summarised in Table S3.† PDO 100 : 0 matches commercial tensile strengths and moduli while printing at 20 μm layers with a 10 s exposure, confirming that the bio-derived ink remains compatible with standard LCD workflows. Overall, the rigid resin performed well in the LCD application and could be used to resolve small features with good clarity.

Molecular influences on resin design

The molecular structure and functionality of the diacid monomers significantly govern the thermal and mechanical attributes of the resulting UV-cured polymer networks. Itaconic acid contains an internal carbon–carbon double bond, while succinic acid is fully saturated. The rigid unsaturated itaconic acid residues reduce chain flexibility and mobility. Additionally, the pendant vinyl groups provide reactive sites to participate in crosslinking during photocuring.

As quantified, increasing the itaconic acid content from 50 to 100 mol% leads to an increase in the double bond density (DBD) of the oligoester species. The higher density of C=C groups enabled additional crosslink formation (Schemes 1 and 2), yielding denser networks with restricted segmental motion as evident from higher Young's modulus and tensile strength (Fig. 4 and Table 2). Consequently, itaconic acid-rich resins displayed enhanced stiffness and strength compared to blends with succinic acid-based samples, although with some loss in ductility. The diacid structure presents an effective means of modulating the resin's mechanical properties. Itaconic acid enhances rigidity and performance for engineering applications requiring dimensionally stable LCD printed parts, while succinic acid provides flexibility when fatigue life or toughness is paramount.

The molecular size and backbone structure of the diol components also influence the mechanical performance of the photocured resin systems. By systematically varying the diol constituents from short 1,2-propanediol to flexible long-chain 1,8-octanediol, the crosslink density, free volume, and relative chain mobility within the polymerized polyesters could be extensively tuned. With increasing diol chain length, the crosslink junctions move further apart, yielding networks with enhanced ductility and impact resilience due to the greater inter-chain spacing and reduced entanglement. Simultaneously, the long alkyl segments provide additional free volume to accommodate molecular fluctuations, decreasing Young's modulus and tensile strength. However, the decline in crosslink density and rigidity leads to compromised strength and elastic modulus. A balance is therefore required between desired stiffness and toughness or durability, depending on application specifications.

The tailored property profiles verify that judiciously selecting the bio-based precursors provides a pathway to meeting diverse mechanical demands. Highly crosslinked stiff resin compositions offer strength for structural applications, whereas flexible networks facilitate devices benefiting from fatigue resistance and conformability. By elucidating structure–processing–property relationships, UV-curable polyester resins with bespoke performance were successfully developed. Overall, the selection of suitable diol precursors enables precise tailoring of the mechanical properties of resins spanning rigid/high-strength to flexible/high-toughness profiles. Using this toolbox of renewable building blocks provides a pathway for developing application-targeted bio-based printing resins to meet diverse additive manufacturing demands.

Conclusions

In summary, we have demonstrated a pathway towards developing sustainable and functional UV-curable bio-based polyester resins for vat polymerization 3D printing applications. By systematically varying the diacid (itaconic acid and succinic acid) and diol (1,2-propanediol, 1,4-butanediol, 1,8-octanediol) precursors, the thermal and mechanical properties of resins could be widely tuned. Favorable processing viscosity profiles were achieved for all resin formulations. Photocuring *via* acrylate groups enabled high gel fractions, confirming excellent crosslinking efficiency. Most notably, the resins' mechanical characteristics spanned a wide range from rigid/high strength formulations to flexible/resilient networks by adjusting bio-based building blocks. Young's moduli ranged over an order of magnitude between 100 and 1000 MPa, while elongation at break varied from 3.5 to 8.5%. Implementation in LCD 3D printing produced intricate sample constructs with exceptional resolution down to 100 μm. Although we demonstrate the tunability of mechanical properties using these systems, work remains related to driving the oligomerization reactions to completion, thereby capping all the carboxylic acid groups in the oligoesters. While we can print with these systems, the presence of these acidic groups in printed objects could be detrimental to an object deployed in an environment that is sensitive to pH. We are investigating these phenomena further.

This work bridges the key gaps linking sustainable resin design to high-performance LCD 3D printing applications. The findings underscore the potential of bio-based polyesters as viable alternatives to traditional petroleum-based resins, offering tunable properties for a wide range of additive manufacturing applications. Further optimization of printable resolutions and investigation of biomedical compatibilities will expand applicability. Overall, the elucidated structure–processing–property framework guides polyester resin advancement for next-generation 3D printing demands.

Author contributions

The manuscript was written through contributions of all authors. All authors have given approval to the final version of the manuscript.

Data availability

The data supporting this article have been included as part of the ESI.†

Conflicts of interest

There are no conflicts to declare.

Acknowledgements

This work was supported by the USDA National Institute of Food and Agriculture and Hatch Appropriations under Project #PEN04869 and Accession #7005684. The authors wish to acknowledge the Penn State Materials Characterization Lab for use of the Bruker Vertex V70 FTIR spectrometer and the MTS Criterion load frame. The authors gratefully acknowledge Dr Tawanda J. Zimudzi for his invaluable assistance with the FTIR measurements and quantitative analysis of the degree of cross-linking. We would also like to acknowledge the support of Dr Christy George and Dr Tapas Mal for their help with collecting NMR spectroscopic data.

References

1 M. Despeisse, F. Mbaye, P. D. Ball and A. Levers, *Prod. Plan. Control*, 2012, **23**, 354–376.
2 U. M. Dilberoglu, B. Gharehpapagh, U. Yaman and M. Dolen, *Procedia Manuf.*, 2017, **11**, 545–554.
3 M. Bifano.
4 F. Zhang, L. Zhu, Z. Li, S. Wang, J. Shi, W. Tang, N. Li and J. Yang, *Addit. Manuf.*, 2021, **48**, 102423.
5 M. Shahbazi and H. Jäger, *ACS Appl. Bio Mater.*, 2021, **4**, 325–369.
6 H. Chen, S.-Y. Lee and Y.-M. Lin, *Polymers*, 2020, **12**, 1500.
7 R. P. Brannigan and A. P. Dove, *Biomater. Sci.*, 2017, **5**, 9–21.
8 Q. Zhang, M. Song, Y. Xu, W. Wang, Z. Wang and L. Zhang, *Prog. Polym. Sci.*, 2021, **120**, 101430.
9 A. M. E. Arefin, N. R. Khatri, N. Kulkarni and P. F. Egan, *Polymers*, 2021, **13**, 1499.
10 T. Robert and S. Friebel, *Green Chem.*, 2016, **18**, 2922–2934.
11 J. Dai, S. Ma, Y. Wu, L. Han, L. Zhang, J. Zhu and X. Liu, *Green Chem.*, 2015, **17**, 2383–2392.
12 S. Bränström, E. Malmström and M. Johansson, *J. Coat. Technol. Res.*, 2017, **14**, 851–861.
13 J. Dai, S. Ma, N. Teng, X. Dai, X. Shen, S. Wang, X. Liu and J. Zhu, *Ind. Eng. Chem. Res.*, 2017, **56**, 2650–2657.
14 X. Dong, J. Ren, Y. Duan, D. Wu, L. Lin, J. Shi, R. Jia, X. Xu and X. He, *Appl. Polym. Sci.*, 2022, **139**, 52042.
15 S. Kumar, S. Krishnan, S. K. Samal, S. Mohanty and S. K. Nayak, *Polym. Int.*, 2017, **66**, 1349–1363.
16 B.-E. Teleky and D. Vodnar, *Polymers*, 2019, **11**, 1035.
17 L. Papadopoulos, N. M. Malitowski, D. Bikiaris and T. Robert, *Eur. Polym. J.*, 2023, **186**, 111872.
18 L. Papadopoulos, L. Malletzidou, D. Patsiaoura, A. Magaziotis, E. Psochia, Z. Terzopoulou, K. Chrissafis, C. Markessini, E. Papadopoulou and D. N. Bikiaris, *Appl. Sci.*, 2021, **11**, 896.
19 K. S. Savitha, B. Ravji Paghadar, M. Senthil Kumar and R. L. Jagadish, *Polym. Chem.*, 2022, **13**, 3562–3612.
20 L. Mitrea, B.-E. Teleky, S.-A. Nemes, D. Plamada, R.-A. Varvara, M.-S. Pascuta, C. Ciont, A.-M. Cocean, M. Medeleanu, A. Nistor, A.-M. Rotar, C.-R. Pop and D.-C. Vodnar, *Heliyon*, 2024, **10**, e25551.
21 V. S. D. Voet, J. Guit and K. Loos, *Macromol. Rapid Commun.*, 2021, **42**, 2000475.
22 E. M. Maines, M. K. Porwal, C. J. Ellison and T. M. Reineke, *Green Chem.*, 2021, **23**, 6863–6897.
23 R. Saraswat, Shagun, A. Dhir, A. S. S. Balan, S. Powar and M. Doddamani, *RSC Sustainability*, 2024, **2**, 1708–1737.
24 J. Guit, M. B. L. Tavares, J. Hul, C. Ye, K. Loos, J. Jager, R. Folkersma and V. S. D. Voet, *ACS Appl. Polym. Mater.*, 2020, **2**, 949–957.
25 M. Lebedevaite, V. Talacka and J. Ostrauskaite, *Appl. Polym. Sci.*, 2021, **138**, 50233.
26 I. Cazin, M. Ocepek, J. Kecelj, A. S. Stražar and S. Schlögl, *Materials*, 2024, **17**, 1890.
27 T. W. Jesse, T. C. Ezeji, N. Qureshi and H. P. Blaschek, *J. Ind. Microbiol. Biotechnol.*, 2002, **29**, 117–123.
28 R. Carmenini, C. Spanu, E. Locatelli, L. Sambri, M. Comes Franchini and M. Maturi, *Prog. Addit. Manuf.*, 2024, **9**, 2499–2510.
29 V. Vetri Buratti, A. Sanz de Leon, M. Maturi, L. Sambri, S. I. Molina and M. Comes Franchini, *Macromolecules*, 2022, **55**, 3087–3095.
30 M. Maturi, C. Pulignani, E. Locatelli, V. V. Buratti, S. Tortorella, L. Sambri and M. C. Franchini, *Green Chem.*, 2020, **22**, 6212–6224.
31 M. Maturi, C. Spanu, E. Maccaferri, E. Locatelli, T. Benelli, L. Mazzocchetti, L. Sambri, L. Giorgini and M. C. Franchini, *ACS Sustainable Chem. Eng.*, 2023, **11**, 17285–17298.
32 L. Papadopoulos, L. Pezzana, N. Malitowski, N. Kladovasilakis, D. Tzetzis, M. Sangermano, D. N. Bikiaris and T. Robert, *Giant*, 2024, **18**, 100275.
33 B. J. Qu and B. Rånby, *Appl. Polym. Sci.*, 1993, **48**, 701–709.
34 F. Wolff, C. Kugler and H. Münstedt, *Rheol. Acta*, 2011, **50**, 917–924.
35 F. Khan, D. Kwek, E. Kronfli and S. R. Ahmad, *Polym. Degrad. Stab.*, 2008, **93**, 1238–1241.
36 L. Papadopoulos, L. Pezzana, N. M. Malitowski, M. Sangermano, D. N. Bikiaris and T. Robert, *ACS Omega*, 2023, **8**, 31009–31020.
37 R. Harikrishna, S. M. Bhosle, S. Ponrathnam and C. R. Rajan, *J. Mater. Sci.*, 2011, **46**, 2221–2228.
38 L. Shen, Y. Wang, Q. Zhao, F. Luo, J. Chen, M. Lu, L. Liang, K. Wu and J. Shi, *Polym. Int.*, 2016, **65**, 1150–1156.
39 D638 standard test method for tensile properties of plastics, **https://www.astm.org/d0638-14.html**, (accessed 2 July 2024).
40 A. M. Herrera-González, M. Caldera-Villalobos, A. A. Pérez-Mondragón, C. E. Cuevas-Suárez and J. A. González-López, *J. Chem. Educ.*, 2019, **96**, 1786–1789.

41 H. R. Allcock, F. W. Lampe and J. E. Mark, in *Contemporary polymer chemistry*, Pearson/Prentice Hall; Pearson Education, Upper Saddle River, N.J., London, 3rd edn, 2003.
42 L. De Keer, P. H. M. Van Steenberge, M.-F. Reyniers and D. R. D'hooge, *Polymers*, 2021, **13**, 2410.
43 M. Fei, T. Liu, B. Zhao, A. Otero, Y.-C. Chang and J. Zhang, *ACS Appl. Polym. Mater.*, 2021, **3**, 2470–2479.
44 J.-T. Miao, S. Peng, M. Ge, Y. Li, J. Zhong, Z. Weng, L. Wu and L. Zheng, *ACS Sustainable Chem. Eng.*, 2020, **8**, 9415–9424.
45 A. R. Rahmat and R. J. Day, *J. Teknol.*, 2012, **39**(1), 83–96.
46 K. Studer, C. Decker, E. Beck and R. Schwalm, *Eur. Polym. J.*, 2005, **41**, 157–167.
47 B. Zhao, C. Hao, Y. Chang, Y. Cao, T. Liu, M. Fei, L. Shao and J. Zhang, *Adv. Funct. Mater.*, 2023, **33**, 2213663.
48 A. T. Deutsch Lukatsky, Y. Dan, L. Mizrahi and E. Amir, *Eur. Polym. J.*, 2024, **210**, 112990.
49 D. Abu-Elenain, S. H. Lewis and J. W. Stansbury, *Dent. Mater.*, 2013, **29**(11), 1173–1181.